Pressure-Induced Molecular Assembly of Hydrogen-Bonded Polymers

SHINGO MUTSUO,[1] KAZUYA YAMAMOTO,[2] TSUTOMU FURUZONO,[3] TSUYOSHI KIMURA,[4] TSUTOMU ONO,[1] AKIO KISHIDA[4]

[1]Department of Material and Energy Science, Graduate School of Environmental Science, Okayama University, Tsushima-Naka, Okayama 700-8530, Japan

[2]Department of Nanostructured and Advanced Materials, Graduate School of Science and Engineering, Kagoshima University, Korimoto, Kagoshima 890-0065, Japan

[3]Department of Biomedical Engineering, National Cardiovascular Center Research Institute, Fujishiro-Dai, Suita, Osaka 565-8565, Japan

[4]Department of Applied Functional Molecules, Institute of Biomaterials and Bioengineering, Tokyo Medical and Dental University, Kanda-Surugadai, Chiyoda-Ku, Tokyo 101-0062, Japan

Received 10 August 2007; accepted 21 December 2007
DOI: 10.1002/polb.21407
Published online in Wiley InterScience (www.interscience.wiley.com).

ABSTRACT: Controlling the noncovalent bondings such as electrostatic interaction, van der Waals force and hydrogen bond, is the key factor to generate molecular assembly. We show that pressure is one of the most intensive variables for controlling these intermolecular forces and producing assembled structure. Macrogel and nanoparticles of hydrogen-bonded polymers were simply obtained through an ultrahigh-pressure process. The morphology of the obtained assembly depends on concentration and various conditions of the pressurization. These results indicate that the ultrahigh-pressure induces inter/intra-hydrogen bond, which is strong enough to maintain microassemblies such as gels and particles. This methodology leads to the molecular design of pressure-induced molecular assembly, and nonharmful processes for molecular separation and drug development. © 2008 Wiley Periodicals, Inc. J Polym Sci Part B: Polym Phys 46: 743–750, 2008
Keywords: crosslinking; hydrogels; nanoparticles; water-soluble polymers

INTRODUCTION

Molecular assembly technology has been gathering interest in the material processing field, especially nanotechnology. Molecular assembly is achieved by noncovalent bonding between adjacent molecules. The development of carbon nanotubes as circuit wires[1,2] and the incorporation of anticancer drugs and amphiphilic polymers into nanomicelles[3,4] are examples of molecular assembly in which noncovalent bonding, such as electrostatic interaction, van der Waals interactions and hydrogen bonds, are well combined.[5–8] Controlling these intermolecular forces is the key factor to create or collapse the assembled structure. Supramolecular chemistry has expanded to allow various elemental molecules to generate elegant assembles,[9–12] whereas the operative factors which regulate molecular assembly are mostly limited by the concentration and/or temperature. Here, we show that

Correspondence to: A. Kishida (E-mail: kishida.fm@tmd.ac.jp)
Journal of Polymer Science: Part B: Polymer Physics, Vol. 46, 743–750 (2008)

pressure, which is one of the most intensive variables in thermodynamics as well as the concentration and temperature,[13–16] can also be used for controlling the intermolecular forces to generate assembled molecules. We found that a poly (vinyl alcohol) (PVA) solution turned into a macrogel or nanoparticle through a simple ultrahigh-pressure process (10,000 atmosphere, 10 min). The morphology of the obtained assembly depended on the PVA concentration, indicating significant inter/intra-molecular hydrogen bonding. Our results demonstrated that ultrahigh-pressure induces hydrogen bonding in water, which is strong enough to maintain microassemblies such as gels and particles.[17,18] Since the interactive potential of molecules is brought out under ultrahigh-pressure, this technology would be applicable to realize the concept for designing assembly molecules proposed by Whitesides and coworkers.[19–21] Furthermore, this methodology leads to the molecular design of pressure-induced molecular assembly, and facilitates nonharmful processes for molecular separation and drug development.

EXPERIMENTAL

Materials

The degree of polymerization of the used PVA (Kuraray, Japan) was 1750. The degree of saponification was 99.8%.

Ultrahigh-Hydrostatic Pressurization

An aqueous PVA solution of predetermined concentration was poured into a plastic bag and was sealed. The bag solution was pressurized using an ultrahigh-pressure machine (hydrostatic pressure). The pressure was set to 1000–10,000 atmospheric pressures, and was processed over the predetermined time period.

Hydrogel Preparation by The Freeze-Thawing Method

An aqueous PVA solution was subjected to five cycles of freeze-thawing, in which the sample was frozen for 12 h at −20 °C, and then thawed for 12 h at 4 °C as one cycle. The mass change of the freeze-thawed sample and the high-pressure processed sample before and after soaking was measured, and the structures of the two gels, both of which had gel ratios over 90%, were compared.

Dynamic Light Scattering Measurement

A 0.5 w/v % PVA solution was high-pressure processed for 10 min at 10,000 atm, and the sample was diluted to an appropriate concentration with ultrapure water, and was subsequently filtered with a 5-μm pore mesh. The particle size was then measured with DLS-7000 (Otsuka Electronics, Japan) using an Ar laser (λ = 488 nm, 75 mW).

Swelling Ratio Measurement

The PVA hydrogel prepared by pressurization was immersed in pure water at room temperature for 10 days and then freeze-dried. The swelling ratio of the PVA hydrogel was calculated as follows:

$$\text{Swelling ratio} = \frac{W_h - W_d}{W_d} \times 100$$

where W_h is the weight of hydrated gel after the dialysis and W_d is the weight of dried gel.

Scanning Electron Microscopy

Observation of PVA assembly was carried out using a scanning electron microscope, S-4700 (Hitachi High Technologies). Specimen for SEM observation was prepared as follows: After a hydrogel was freeze-dried, it was coated with a thin layer of Pt–Pd by the vacuum evaporation technique.

Differential Scanning Calorimetry

DSC measurement was carried out to reveal the melting temperature of PVA assembly. It was carried out at heating rate of 5 °C/min under a constant flow of nitrogen gas.

^{1}H NMR Measurement

The nongelled portion of the pressurized PVA was obtained by the dialysis of the PVA hydrogel. The ^{1}H NMR spectra was obtained by the measurement of the PVA sample dissolved in dimethyl sulfoxide (DMSO-d_6).

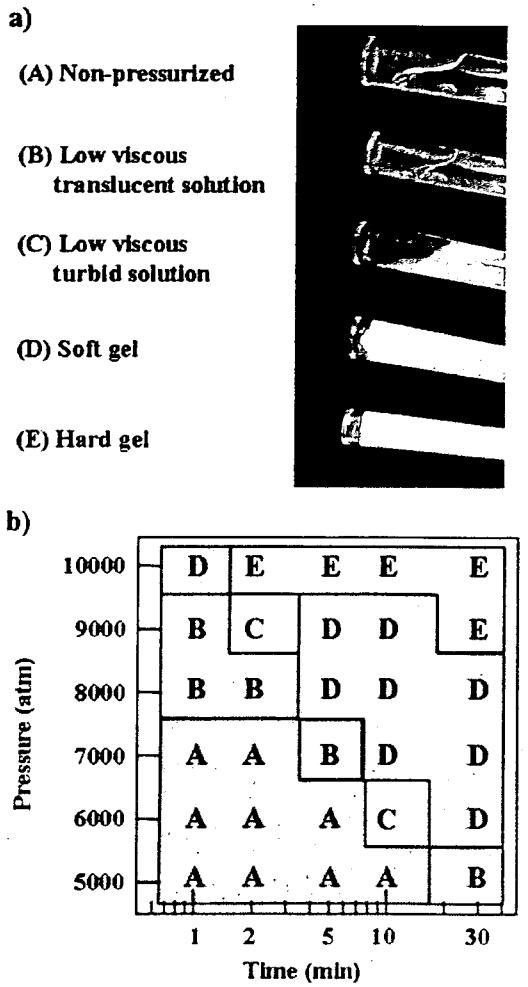

Figure 1. Pressure-induced PVA assembly. (a) Photographs of a 10 w/v% PVA solution pressurized under various conditions: (A) nonpressurized, (B) 7000 atm, 1 min, (C) 9000 atm, 1 min, (D) 7000 atm, 10 min, and (E) 10000 atm, 10 min. (b) Phase (constitutional) diagram of a 5 w/v % PVA solution pressurized under various conditions. The state was decided by visual observation according to the photographs. [Color figure can be viewed in the online issue, which is available at www.interscience.wiley.com.]

RESULTS AND DISCUSSION

PVA Assembly Formed by Pressurization

Aqueous solutions of PVA at 1–20 w/v % concentrations were pressurized hydrostatically under various conditions. Figure 1(a) shows photographs of typical samples of 10 w/v % PVA solutions pressurized at different atmosphere pressure (atm) for 10 min. A translucent solution, the precipitate and hydrogel of PVA was obtained by increasing the pressure, indicating that the assembly of PVA molecules was induced by pressure treatment. The hydrogel was stable in pure water, and the yield (gelation ratio) was 90% or more. It is well-known that PVA solutions transform into hydrogels when the solution was frozen and thawed sequentially several times; this procedure is called the freeze-thawing method. Approximately 10 days is required to form a hydrogel with similar strength as a hydrogel obtained by pressurization for only 10 min. Thus, this simple pressurizing method can be expected to be an energy saving process. The influence of the pressure conditions on the formation of a PVA assembly was examined using a PVA solution of 5 w/v % in detail. Figure 1(b) shows the state diagram of the PVA assembly in a pressure–time plot determined by visual observation according to the photographs shown in Figure 1(a). The translucent solution and hydrogel were acquired by pressure treatment at more than 8000 atm over a very short time (one min). The tendency for gelation of PVA with increasing pressure was observed for each step of pressurization. In addition, at constant pressure, a long period of pressure treatment induced assembly of the PVA, even in the case of only 6000 atm, and the hydrogel was obtained by pressurization for 30 min. Furthermore, DLS measurements of a 10 w/v % solution pressurized under conditions in which a hydrogel was not obtained revealed the formation of PVA nanoassembly and the

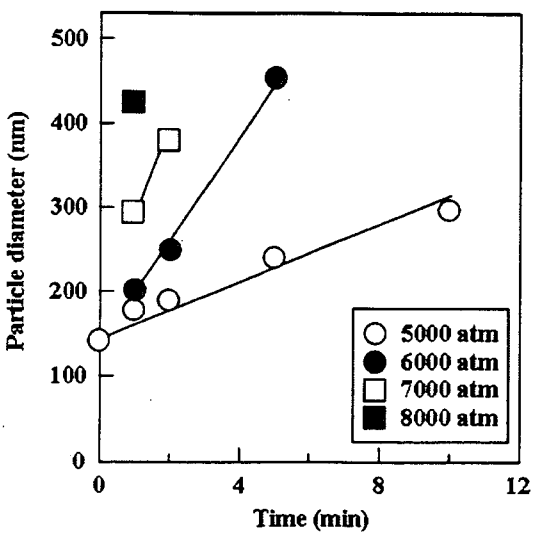

Figure 2. DLS measurements of a 10 w/v % PVA solution pressurized under various conditions.

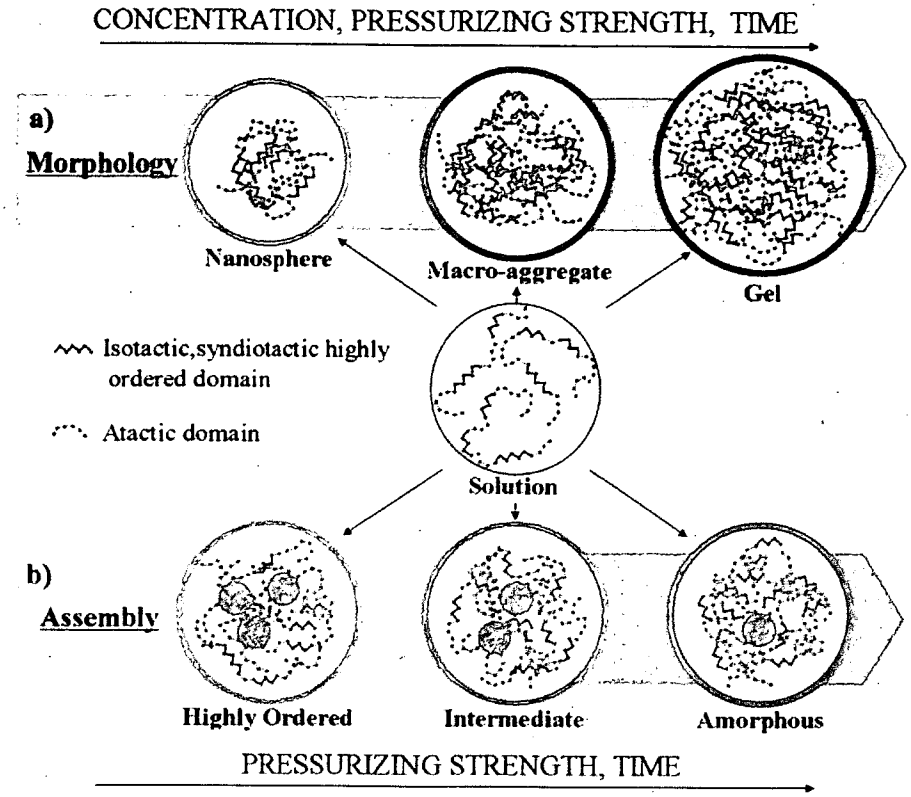

Figure 3. Illustration of the mechanism of hydrogen-bonding polymer assembly induced by ultrahigh-pressurization. (a) Effect of conditional parameters on the morphology of PVA assembly. (b) Effect of secondary structure of PVA on the formation of molecular assembly.

growth of the PVA nanoassembly under prolonged periods of pressure (Fig. 2). From these results, it is clear that the assembly of PVA at nanometer size was promoted under pressure conditions of higher pressure and a longer incubation period, and could be controlled by altering the pressurizing strength and time [Fig. 3(a)].

Characteristics of PVA Assembly Formed By Pressurization

The gelation of a PVA solution at 5, 10, 15, and 20 w/v % concentrations was also achieved by pressurization at 10,000 atm. The swelling ratio of the obtained hydrogel was determined by the starting concentration of the PVA solution, and showed a constant value for all concentrations when they were treated at 10,000 atm for more than 10 min (Fig. 4). On the other hand, the swelling ratio of the obtained hydrogel at 5 min of pressurizing time was inversely proportional to the concentration of the PVA solution (Fig. 5). This result indicates that a tight interaction

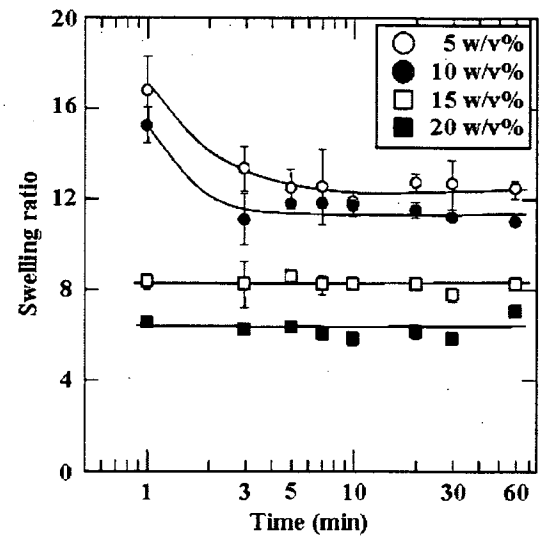

Figure 4. Effect of PVA concentration on swelling ratio of PVA hydrogel formed by pressurization at 10,000 atm for various minutes.

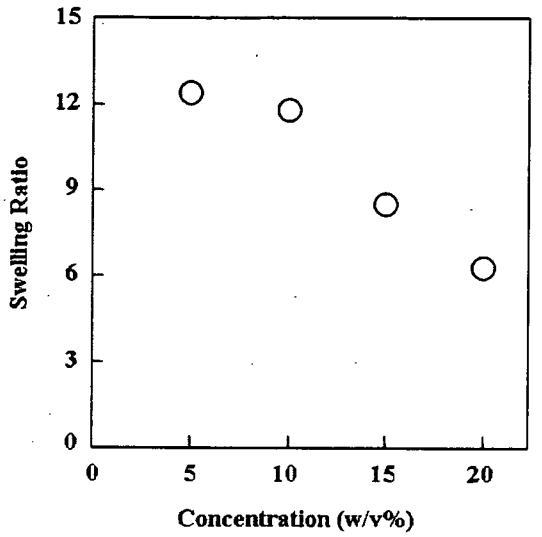

Figure 5. Swelling ratio of PVA hydrogels formed by pressurization at 10,000 atm for 5 min.

between the PVA molecules was formed with increasing the concentration of PVA solution. The interior structure of the PVA hydrogel pressurized at 10,000 atm for 10 min was observed with a SEM (Fig. 6). A mesh-like structure with pores of about 300 nm was observed for the hydrogel obtained by the pressure treatment of a 5 w/v % PVA solution. The mesh-like structures with smaller pores were formed upon increasing the PVA concentration. As the pressure treatment was carried out at 40 °C, no ice crystal was formed.[22] That is, ice crystals did not affect the mesh-like structures formed by the high-pressure process. In contrast, in the case of the freeze-thawing method, the mesh-like structures were formed by the formation of ice crystals. Therefore, a different process of formation between the two methods was suggested.

DSC analysis of the PVA hydrogels let us know the melting temperature of the associated PVA molecules. The relaxation, which occurs at a temperature between 200 and 260 °C, is caused by the melting of the crystalline domains of PVA.[23,24] The increase of intermolecular hydrogen bonding in PVA raises the melting temperature, leading to a high heat resistance.[25] The melting temperature of the PVA hydrogel

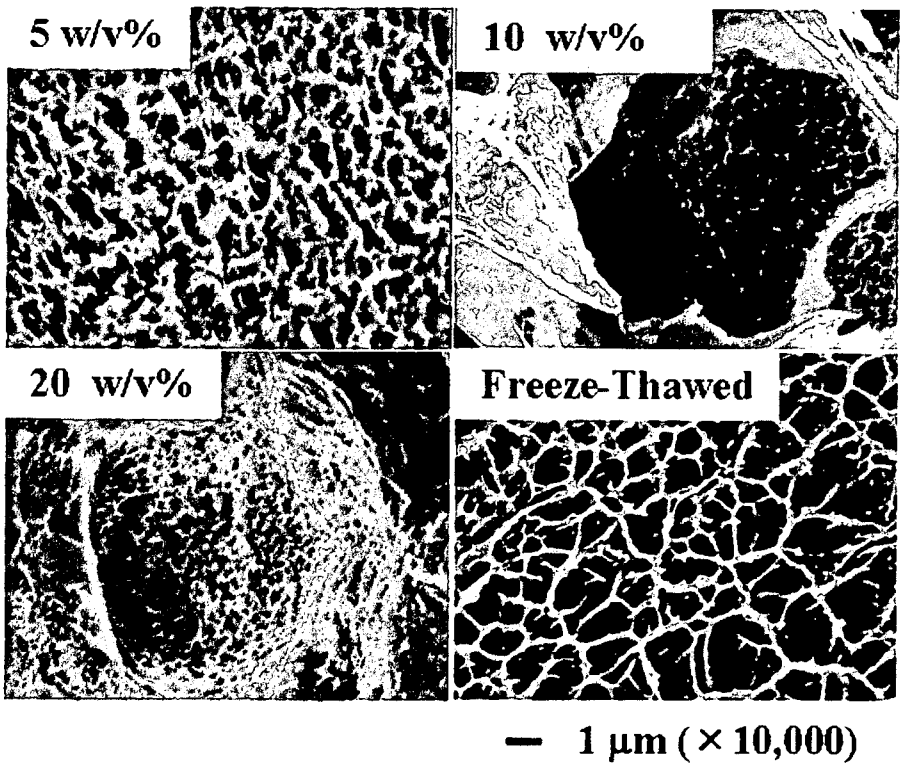

Figure 6. SEM images of PVA hydrogels of 5, 10, and 20 w/v % formed by pressurization at 10,000 atm for 10 min and 5 w/v % PVA hydrogels formed by the freeze-thawing method.

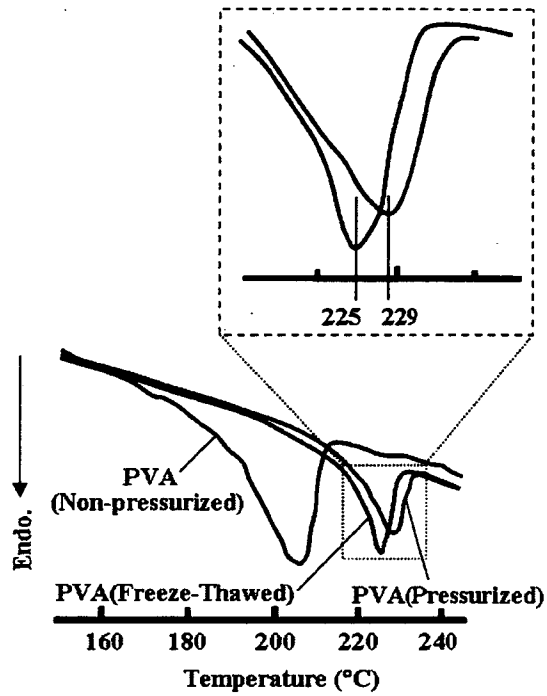

Figure 7. DSC measurements of PVA hydrogels formed by pressure treatment or the freeze-thawing method.

obtained by high-pressure process was higher than that of the hydrogel prepared by the freeze-thawing method (Fig. 7). This result indicates that high-pressure process could form stronger intermolecular interactions in PVA than the freeze-thawing method. Although we need to go into additional details about the thermodynamic stability of the PVA hydrogel obtained by high-pressure process, we have only limited information about it.

Many researchers have examined the self-organization of molecules in an aqueous environment, because the hydrogen bonds and hydrophobic interactions were able to act as a driving force for structure formation.[26–29] The formation and deformation of the hydrogen bonds in an aqueous environment can be controlled by changing the temperature and ionic concentration. The effect of the salt concentration on the high-pressure process of the PVA solution was then examined. When the NaCl concentration was increased, the PVA hydrogel was obtained even at low pressure (around 6000 atm). At over 9000 atm, stable PVA hydrogels were obtained at any salt concentration, and the swelling ratio was almost constant (Fig. 8).

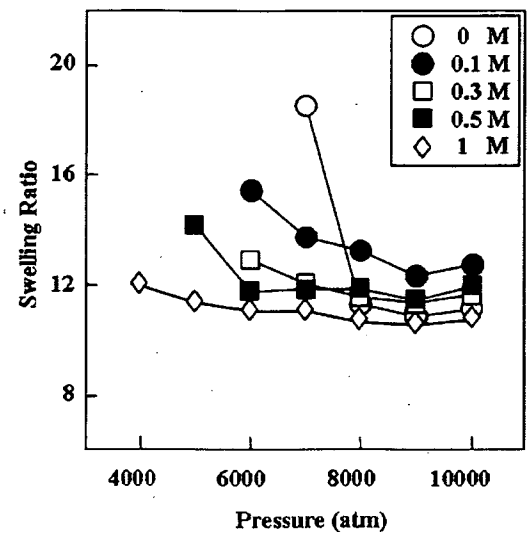

Figure 8. Swelling ratio of 10 w/v% PVA hydrogels formed by pressurization at 10,000 atm for 5 min with various salt concentrations.

When PVA solutions of less than 1 w/v % concentration were treated with pressurization at 10,000 atm, clear and turbid solutions were obtained, as well as in the case of a 10 w/v % PVA solution pressurized under low atmospheric pressure for a short time. The formation of small particles with a diameter of about 200–400 nm was confirmed from SEM observation and DLS measurements (Fig. 9). As a result, it was believed that the formation of intra/inter-molecular hydrogen bonds is the first step in the initial structural formation of PVA, and afterward the size and morphology of the structure is determined in proportion to the concentration of the solution.

The effect of the secondary (atactic, syndiotactic, and isotactic) structure of PVA molecule was observed by the ^{1}H NMR spectra analysis for the nongelled portion of the pressurized PVA solution (Table 1). Short-time pressurizing treatment at

Table 1. NMR Analysis of the Nongelled Portion of the Pressurized PVA Solution

	Tacticity		
	mm	mr	rr
PVA117HC	22.6	47.6	29.8
S-PVA	11.9	49.9	38.2
PVA117HC (20%, 6000 atm, 5 min)	21.4	49.0	29.6
PVA117HC (20%, 6000 atm, 10 min)	33.8	37.7	28.5
PVA117HC (10%, 7000 atm, 5 min)	20.9	48.0	31.1

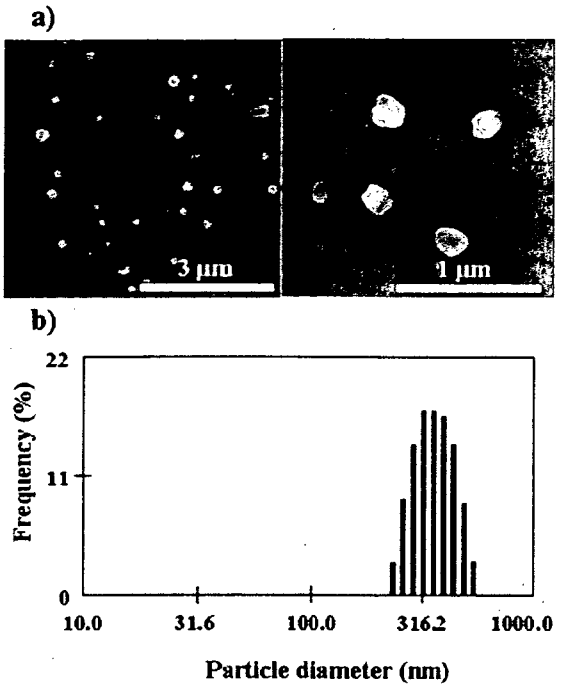

Figure 9. Small aggregates formation of PVA by pressurization. (a and b) SEM images and DLS measurements, respectively, of PVA particles formed by pressurizing a 0.5 w/v % PVA solution at 10,000 atm for 10 min.

6000 atm had no effect on the content of the secondary structure of PVA molecule, whereas after the longer treatment (10 min), the decrease of the atactic portion (mr) of PVA molecule was observed. There was no free PVA after more than 20-min treatment. These results indicated that the atactic PVA was gelled prior to other kinds of the stereostructured PVA, and after prolonged treatment all kinds of stereostructured PVA gelled. These differences of aggregation ability of each stereostructured PVA could be applicable to form the ordered structure by changing treatment time, pressure, and the content of each secondary structures of PVA [Fig. 3(b)].

The High-Ordered Structure of PVA Assembly

The assembly of PVA depended on the strength and period of pressurization and the PVA concentration. It should be noted that molecular assembly is formed through two processes induced by pressurization, which are dehydration and the subsequent formation of hydrogen bonds among inter/intra-molecules. Indeed, it is believed that under pressurized conditions, the hydration shell of the PVA molecules was disrupted, and then hydrogen bonding interactions between the hydroxyl groups of the PVA were formed. Thus, the gelation of PVA was promoted by increasing the pressure. It seems that the reaction could proceed with a long duration of pressurization even at moderate pressures. With regard to the concentration-assembly relationship, monodispersed and nanometer-scale structures were formed by intramolecular interactions under dilute conditions, whereas the macrostructure (larger than mm) was formed by the intermolecular interactions between nanometer-scaled structures which contained molecular entanglements under concentrated conditions. To construct a well-defined molecular assembly, it is necessary to optimize the primary chemical structure of the polymer molecules, and to fabricate molecules with a specific structure by exploiting various interactions. The intermolecular force maintaining the structure of the supramolecular assembly includes van der Waals force, electrostatic interactions, hydrophobic interactions, and hydrogen bonds, etc. The individual interaction energy of a hydrogen bond is small, while if it interacts along the chain direction, hydrogen bond is able to maintain a huge PVA hydrogel by assembling high-molecular weight PVA moieties. The most important factor that influences the structure formation induced by high pressure is the chain length and the secondary structure of the PVA molecule, as well as the temperature, concentration, and ionic concentration. Controlling the factors, it is expected that the ordered structures of molecular assembly can be generated. In a conventional technique, changing the concentration of the solution or a substitution of the solvent makes it difficult to change the molecular-assembly situation gradually. On the other hand, the pressuring conditions can be reversibly controlled and highly controlled operation for molecular assembly by building the interactive part, which works at a different pressure in the molecules. In the case where two or more hydrogen bonding functional groups are present, the control of a higher-order structure can be achieved by pressurizing in a stepwise fashion. We assumed that the secondary structure of PVA is one of the most possible candidates for the factors for obtaining the ordered molecular assembling structure. It is expected that such technology can be applied to build a structure by the manipulating molecular interactions to develop

novel structure in aqueous solution, leading to new science and technology.

CONCLUSIONS

The PVA assembly was simply obtained through an ultrahigh-pressure process. The morphology of PVA assembly depended on the strength and period of pressurization, the PVA concentration, the PVA chain length, and the PVA secondary structure. Under the ultrahigh-pressure, molecular assembly is formed through two processes, which are dehydration and the subsequent formation of hydrogen bonds among inter/intramolecules. Thus, the ultrahigh-pressure process can manipulate molecular interactions. Therefore, it is expected that the novel high-ordered structures based on molecular assembly can be generated by controlling various factors in an ultrahigh-pressure process.

This work was partly supported by Kuraray Co., for their supply of the poly(vinyl alcohol).

REFERENCES AND NOTES

1. Joachim, C.; Gimzewski, J. K.; Aviram, A. Nature 2000, 408, 541–548.
2. Cui, Y.; Lieber, C. M. Science 2001, 291, 851–853.
3. Yokoyama, M.; Miyauchi, M.; Yamada, N.; Okano, T.; Sakurai, Y.; Kataoka, K.; Inoue, S. Cancer Res 1990, 50, 1693–1700.
4. Nishiyama, N.; Kataoka, K. Pharmacol Ther 2006, 112, 630–648.
5. Bong, D. T.; Clark, T. D.; Granja, J. R.; Ghadiri, M. R. Angew Chem Int Ed 2001, 40, 988–1011.
6. Chandler, D. Nature 2005, 437, 640–647.
7. Tanaka, T.; Tasaki, T.; Aoyama, Y. J Am Chem Soc 2002, 124, 12453–12462.
8. Zemb, T. Curr Opin Colloid Interface Sci 2003, 8, 1–4.
9. Lehn, J. M. Proc Natl Acad Sci USA 2002, 99, 4763–4768.
10. Prins, L. J.; De Jong, F.; Timmerman, P.; Reinhoudt, D. N. Nature 2000, 408, 181–184.
11. Barth, J. V.; Weckesser, J.; Lin, N.; Dmitriev, A.; Kern, K. Appl Phys A: Mater Sci Process 2003, 76, 645–652.
12. Balzani, V.; Credi, A.; Raymo, F. M.; Stoddart, J. F. Angew Chem Int Ed 2000, 39, 3348–3391.
13. Mozhaev, V. V.; Heremans, K.; Frank, J.; Masson, P.; Balny, C. Proteins: Struct Funct Genet 1996, 24, 81–91.
14. Kunugi, S.; Yoshida, D.; Kiminami, H. Colloid Polym Sci 2001, 279, 1139–1143.
15. Otero, L.; Sanz, P. D. J Food Sci 2003, 68, 2523–2528.
16. Kalichevsky-Dong, M. T.; Ablett, S.; Lillford, P. J.; Knorr, D. Int J Food Sci Technol 2000, 35, 163–172.
17. Kunugi, S.; Takano, K.; Tanaka, N.; Suwa, K.; Akashi, M. Macromolecules 1997, 30, 4499–4501.
18. Seto, Y.; Kameyama, K.; Tanaka, N.; Kunugi, S.; Yamamoto, K.; Akashi, M. Colloid Polym Sci 2003, 281, 690–694.
19. Bowden, N.; Terfort, A.; Carbeck, J.; Whitesides, G. M. Science 1997, 276, 233–235.
20. Breen, T. L.; Tien, J.; Oliver, S. R. J.; Hadzic, T.; Whitesides, G. M. Science 1999, 284, 948–951.
21. Whitesides, G. M.; Crzybowski, B. Science 2002, 295, 2418–2421.
22. Chou, I. M.; Blank, J. G.; Goncharov, A. F.; Mao, H. K.; Hemley, R. J. Science 1998, 281, 809–812.
23. Nugent, M. J. D.; Higginbotham, C. L. Eur J Pharm Biopharm 2007, 67, 377–386.
24. Hassan, C. M.; Ward, J. H.; Peppas, N. A. Polymer 2000, 41, 6729–6739.
25. Nagara, Y.; Nakano, T.; Okamoto, Y.; Gotoh, Y.; Nagura, M. Polymer 2001, 42, 9679–9686.
26. Arnaud, A.; Belleney, J.; Boue, F.; Bouteiller, L.; Carrot, G.; Wintgens, V. Angew Chem Int Ed 2004, 43, 1718–1721.
27. Kim, C.; Lee, S. J.; Lee, I. H.; Kim, K. T.; Song, H. H.; Jeon, H. J. Chem Mater 2003, 15, 3638–3642.
28. Kawasaki, T.; Tokuhiro, M.; Kimizuka, N.; Kunitake, T. J Am Chem Soc 2001, 123, 6792–6800.
29. Roy, S.; Dey, J. Langmuir 2003, 19, 9625–9629.

CHEMMEDCHEM

DOI: 10.1002/cmdc.200700265

Reduction of Lipophilicity at the Lipophilic Domain of RXR Agonists Enables Production of Subtype Preference: RXRα-Preferential Agonist Possessing a Sulfonamide Moiety

Kayo Takamatsu,[a] Atsushi Takano,[a] Nobumasa Yakushiji,[a] Ken-ichi Morishita,[a] Nobuyasu Matsuura,[b] Makoto Makishima,[c] Hamed Ismail Ali,[d] Eiichi Akaho,[d] Akihiro Tai,[a] Kenji Sasaki,[a] and Hiroki Kakuta*[a]

*Retinoid X receptor agonists (RXR agonists, rexinoids) are interesting candidates for the treatment of cancers such as tamoxifen-resistant breast cancer and taxol-resistant lung cancer. However, well-known RXR agonists possess a strong lipophilic character. In addition, although RXR has three subtypes, no subtype-selective RXR agonists are known. Thus we aimed to produce less-lipophilic and subtype-selective RXR agonists. By designing sulfonamide-type RXR agonists, 4-[N-methanesulfonyl-N-(5,5,8,8-tetramethyl-5,6,7,8-tetrahydro-2-naphthyl)amino]benzoic acid (**8a**) was found to prefer RXRα over RXRβ and RXRγ, although the potency is less than the potencies of well-known RXR pan-agonists. Moreover, our results suggest that the reduction of lipophilicity at the hydrophobic interaction region of RXR agonists enables production of RXR subtype preference. Our finding will be useful for the creation of more potent and less-lipophilic subtype-selective RXR agonists aimed at the reduction of undesirable side effects.*

Introduction

Nuclear receptors, which are derived from a common primordial gene, are ligand-dependent transcription factors.[1,2] There are 48 distinct nuclear receptors in humans which are classified into two types. One type comprises the receptors with known endogenous ligands, such as retinoic acid, vitamin D, thyroid hormone, steroid hormones, and/or lipids. The other type are orphan receptors whose functions have not been determined.[1,3] Nuclear receptors work as monomers or dimers by themselves or with other partners. Representative nuclear receptors that function as homodimers or heterodimers are retinoid X receptors (RXRs), whose endogenous ligands are 9-*cis*-retinoic acid (9-*cis*RA; **1**)[4] and docosahexaenoic acid (DHA; **2**)[5] (Figure 1).

The heterodimeric partners of RXRs contain retinoic acid receptors (RARs) that regulate cell differentiation and proliferation, vitamin D receptor (VDR) associated with bone metabolism, peroxisome proliferator-activated receptors (PPARs) associated with lipid metabolism, thyroid hormone receptors (TRs) involved with basal metabolites, and pregnane X receptors

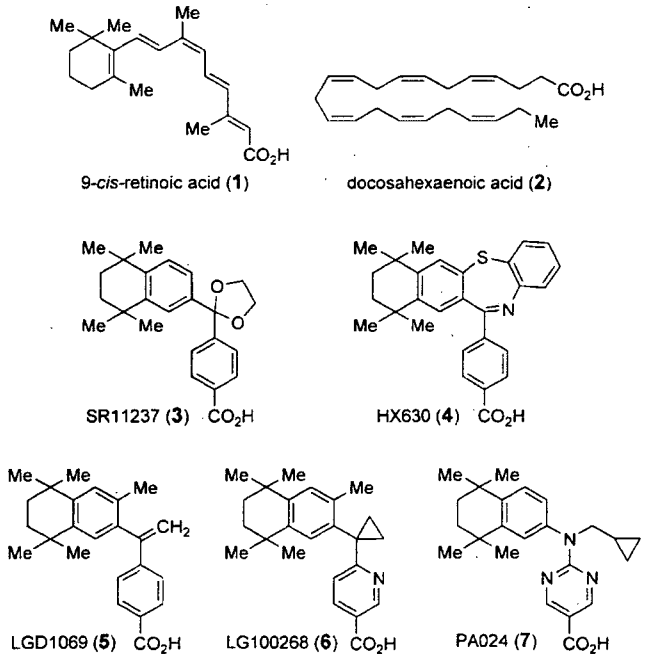

Figure 1. Chemical structures of known endogenous (**1**, **2**) and synthetic (**3**–**7**) RXR agonists.

[a] *K. Takamatsu, A. Takano, N. Yakushiji, K.-i. Morishita, Prof. A. Tai, Prof. K. Sasaki, Prof. H. Kakuta*
Okayama University Graduate School of Medicine
Dentistry and Pharmaceutical Sciences
1-1-1, Tsushima-Naka, Okayama 700-8530 (Japan)
Fax: (+81) 86-251-7926
E-mail: kakuta@pharm.okayama-u.ac.jp

[b] *Prof. N. Matsuura*
Faculty of Science, Okayama University of Science
1-1, Ridai-cho, Okayama 700-0005 (Japan)

[c] *Prof. M. Makishima*
Division of Biochemistry, Department of Biomedical Sciences
Nihon University School of Medicine
30-1 Oyaguchi-kamicho, Itabashi-ku, Tokyo 173-8610 (Japan)

[d] *H. I. Ali, Prof. E. Akaho*
Faculty of Pharmaceutical Sciences
High Technology Research Center (Life Science Center)
Kobe Gakuin University
518 Arise, Ikawadani-cho, Nishi-ku, Kobe 651-2180 (Japan)

(PXRs) associated with expression of CYP3A4 involved in drug metabolism.[1] Therefore, RXRs are closely linked to the function of their partners, and RXR modulators enable control of the function of RXR heterodimeric partners.[6]

RXR agonists can act synergistically with partners. For example, when RXR agonists are treated with RAR agonists (so-called "retinoids", which are known as cell differentiation inducers), cell differentiation occurs typically at subefficacious concentration of RAR agonists alone.[7,8] Similar synergistic activities of RXR agonists are expected for those of other RXR heterodimeric partners such as VDR or PPARs.[6] Some RXR agonists (for example, LGD1069) have recently been used in clinical trials for the treatment of cancers such as tamoxifen-resistant breast cancer[9] and taxol-resistant lung cancer.[10] However, such RXR agonists possess a strong lipophilic character (Figure 1 and Table 1). A problem for clinical application would, therefore, be the possibility of undesirable side effects caused by the high lipophilicity. To prevent this problem, we decided to try to produce new RXR agonists whose lipophilicity are diminished.

Table 1. Calculated log *P* (Clog *P*) values of known RXR agonists.

Compd.:		3	4	5	6	7
Clog *P*	[a]	6.45	9.22	8.23	7.44	7.23
	[b]	5.92	8.31	6.81	5.37	5.02

[a] Calculated with ChemDraw Ultra 7.0. [b] Calculated with molinspiration (http://www.molinspiration.com)

RXR possess three different subtypes, RXRα, RXRβ, and RXRγ. RXRα is expressed mainly in the liver, kidney, and spleen, RXRβ is ubiquitously distributed, and RXRγ is expressed mainly in skeletal muscles, heart muscle, skin, and brain.[11] Nonetheless, no subtype-selective RXR agonists are known.[12,13] These facts encouraged us to develop less-lipophilic and subtype-selective RXR agonists. In this article, molecular design, synthesis, and bioactive assay of our new RXR agonists are reported.

Results and Discussion

To develop subtype-selective RXR agonists, we examined the information available. There is no apparent difference between the amino acid sequences in the ligand-binding domain of each RXR subtype.[14] Thus, activity and potency of various known RXR agonists for each subtype was examined in detail. PA024 (**7**) tends to act more potently toward RXRα/γ than RXRβ, which was not discussed in the previous report.[15] A comparison of the differences between characteristics of PA024 (**7**) and those of other known RXR agonists revealed that the Clog *P* value (a lipophilicity index) of PA024 (**7**) was lower than that of other compounds (Table 1). Highly lipophilic molecules tend to bind proteins nonspecifically. Thus, we hypothesized that less-lipophilic RXR agonists may acquire subtype specificity. This approach was judged to make it possible to reach our dual-purpose.

For designing less-lipophilic RXR agonists, we focused on a sulfonamide group, which possesses a polar character and is seen in many drugs, for example, sulfa drugs. Hence, a sulfonamide group was introduced into the "linking group" that connects the "acidic domain" and the "hydrophobic domain" of the generic RXR pharmacophore described in Figure 2.

Synthesis was performed as described in Scheme 1. After the preparation of tetrahydrotetramethylnaphthylamine (**11**) according to the reported method,[7] compounds **8a–d**, whose acidic domain is a benzoic acid, were synthesized by coupling reaction with ethyl 4-iodobenzoate using $Pd_2(dba)_3$ as a catalyst. After treatment with NaH in anhydrous DMF, the reaction mixture was treated with the corresponding alkylsulfonyl chloride to give sulfonamide ester intermediates. Deprotection of these esters was performed in an alkaline condition to afford the objective compounds **8a–d**.

Compound **9**, whose acidic domain is a nicotinic acid, was synthesized via the amino intermediate **13** by coupling reaction of amine (**11**) with 6-chloronicotinic acid in acetic acid under reflux. Compound **10**, whose acidic domain is a pyrimidine-5-carboxylic acid, was prepared via the amino intermediate **14** according to the reported method.[15,16] Then sulfonamidation and ester deprotection of compounds **13** and **14** was performed by the same procedure as that used for compounds **8a–d** to afford the objective compounds **9** and **10**, respectively.

RXR agonists, when combined with RAR agonists, induce cell differentiation in a synergistic fashion compared to RXR or RAR agonists (for example, Am80[7]) used alone. Cell differentiation can be observed using nitro blue tetrazolium (NBT) reduction.[13,17,18] We have tested compounds **8a–d**, **9**, and **10** for their ability to induce cell differentiation as a single agent or in combination with Am80. Table 2 shows retinoid or retinoid synergistic activities of our compounds and PA024 (**7**). None of the compounds **8a–d**, **9**, and **10** exhibited retinoid activity, suggesting they are not RAR agonists. A marked synergistic activity was observed with **8a**, **9**, and **10**, however with a reduced potency and efficacy compared to PA024 (**7**). Interest-

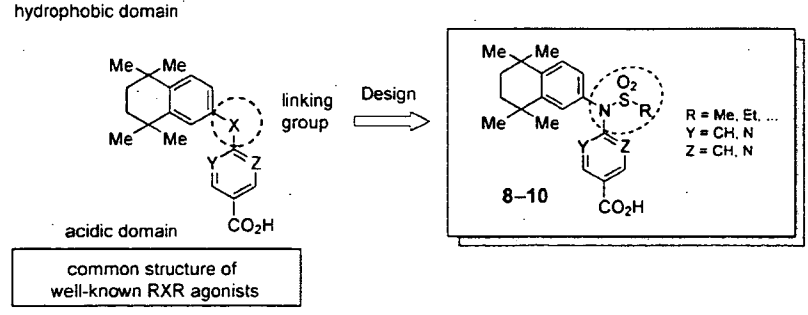

Figure 2. Strategy for the molecular design of low-lipophilic RXR agonists possessing sulfonamide moieties (**8–10**).

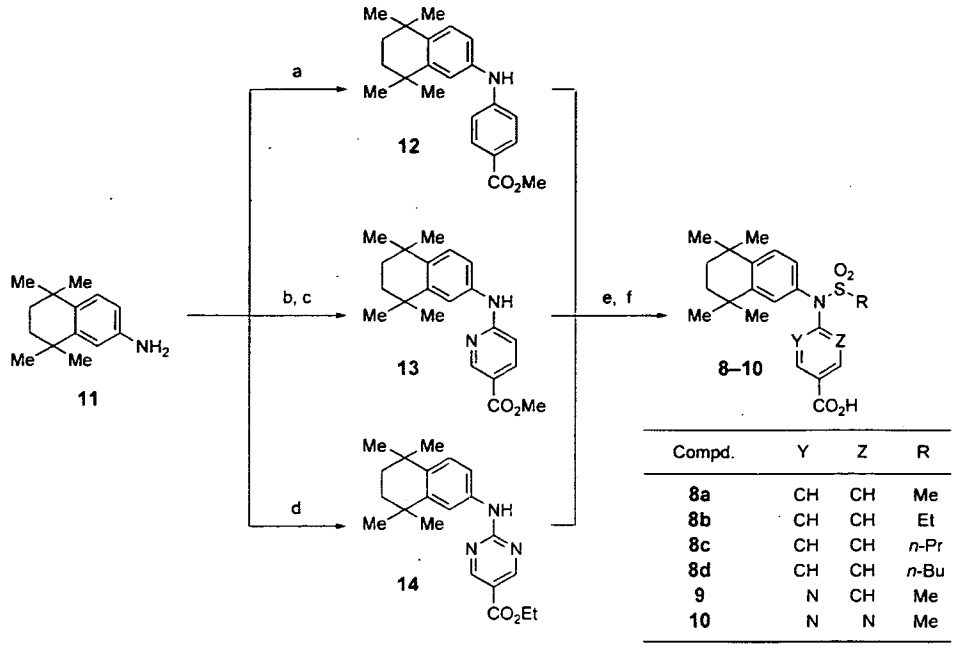

Compd.	Y	Z	R
8a	CH	CH	Me
8b	CH	CH	Et
8c	CH	CH	*n*-Pr
8d	CH	CH	*n*-Bu
9	N	CH	Me
10	N	N	Me

Scheme 1. Reagents and conditions: a) methyl-4-iodobenzoate, BINAP, $Pd_2(dba)_3$, Cs_2CO_3, toluene; b) 6-chloronicotinic acid, AcOH; c) MeOH, H_2SO_4; d) ethyl-2-chloro-5-pyrimidinecarboxylate, K_2CO_3, DMF; e) RSO_2Cl, NaH, DMF; f) LiOH, H_2O, THF.

Table 2. Cell differentiation inducing activity of compounds **8–10**, determined by NBT reduction assay.[a]

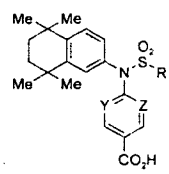

Compd.	R	Y	Z	Retinoid activity		Retinoid synergist activity	
				EC_{50}[b] [nM]	BA[c] [%]	EC_{50}[b] [nM]	BA[c] [%]
8a	Me	CH	CH	> 10000	2 ± 0	300 ± 30	67 ± 5
8b	Et	CH	CH	Inactive	–	830 ± 10	42 ± 0
8c	*n*-Pr	CH	CH	Inactive	–	Inactive	–
8d	*n*-Bu	CH	CH	Inactive	–	Inactive	–
9	Me	N	CH	> 10000	4 ± 1	150 ± 10	73 ± 1
10	Me	N	N	> 10000	1 ± 0	2200 ± 200	56 ± 0
PA024 (**7**)				Inactive	–	3.3 ± 0.6	83 ± 1

[a] All values were determined from full dose-response curves ranging from 10^{-9} to 10^{-5} M with HL-60 cells. Where errors are indicated, values represent the standard error of the mean value of at least two separate experiments. [b] EC_{50} was determined as the concentration of a test compound that was required to elicit a response at half-maximal height on the dose-response curve. [c] Biological activity (%) is maximal differentiation ratio that was induced by a test compound.

ingly, not showing retinoid synergistic activity, compounds **8c** and **8d** indicated a tendency to inhibit compound **9**-induced-retinoid synergistic activity (data not shown).

Next, these compounds were assayed for luciferase transcription activities by a reporter gene assay[15,19,20] to compare their potencies toward each RXR subtype. As SR11237[21] (**3**) possesses polar cyclic acetal moiety, the Clog*P* value was thought to be low and show subtype-preference (activity toward RXRα was only reported). Table 3 shows EC_{50} and E_{max} values in each RXR subtype and Clog*P* values of compounds **8a–d**, **9**, **10**, SR11237 (**3**), LGD1069[22] (**5**), and PA024 (**7**). All tested compounds showed transcription activities, indicating that their retinoid synergistic activities were mediated by RXR. Compounds **8b–d** showed weak RXR agonist activities, as expected from the results of the NBT assay. Notably, compounds **8a**, **9**, and SR11237 (**3**) showed lower Clog*P* values than LGD1069 (**5**) and an apparent difference in EC_{50} between each subtype. The ratio of EC_{50} values between RXRα:RXRβ:RXRγ for LGD1069 (**5**) was 1.0:2.0:1.6, in contrast, that for PA024 (**7**) was 1.0:8.0:2.6. SR11237 (**3**) shows that the ratio of EC_{50} values between RXRα:RXRβ:RXRγ was 1.0:3.3:9.0. For compound **8a**, the ratio of EC_{50} values between RXRα:RXRβ:RXRγ was 1.0:11.5:3.1, indicating that this compound prefers RXRα/γ over RXRβ. Considering the fact that the E_{max} value of **8a** toward RXRα is larger than that of RXRβ or RXRγ by 50%, compound **8a** can be regarded as an RXRα-preferential agonist. SR11237 (**3**), PA024 (**7**), compounds **8a**, and **9** show lower Clog*P* values than LGD1069 (**5**) and subtype-preference, supporting our hypothesis that less-lipophilic RXR agonists are able to produce RXR subtype selectivity. In contrast, compound **10**, whose Clog*P* value is the lowest in this study,

Table 3. Co-transfection data for compounds **8–10** and known RXR agonists (**3**, **5**, and **7**).[a]

Compd.	RXRα		RXRβ		RXRγ		Clog P[d]
	EC_{50}[b] [nM]	E_{max}[c] [%]	EC_{50}[b] [nM]	E_{max}[c] [%]	EC_{50}[b] [nM]	E_{max}[c] [%]	
8a	195±25	115±16	2250±0	52±14	620±50	59±3	6.55
8b	307±1	79±1	2009±579	102±4	1254±431	112±3	7.08
8c	2019±203	71±7	1452±452	24±11	2347±530	73±32	7.61
8d	2795±112	33±10	2201±868	28±11	2397±239	17±4	8.14
9	115±5	98±6	635±75	94±2	350±85	81±7	6.17
10	1888±488	147±7	1995±394	84±6	1519±130	42±6	5.46
SR11237 (**3**)	29±3	111±8	98±27	106±7	232±82	122±4	6.45
LGD1069 (**5**)	3±0	106±12	6±1	114±12	5±2	104±3	8.23
PA024 (**7**)	3±1	100	24±0	100	8±1	100	7.23

[a] All values represent the standard error of the mean value of at least two separate experiments with triplicate determinations. [b] EC_{50} values were determined from full dose-response curves ranging from 10^{-9} to 10^{-5} M in COS-1 cells. [c] Luciferase activity of PA024 (**7**) at 1 μM was defined as 100%. [d] Clog P values were calculated with ChemDraw Ultra 7.0.

showed lower subtype-preference and potency than compound **8a**. Considering this result, we are proposing that production of subtype-preference, reduction of lipophilicity should be performed at the lipophilic domain of RXR agonists rather than at the acidic domain.

To understand the reason why compound **8a** shows subtype preference, a docking study was performed with AutoDock.[23] Unfortunately, no apparent differences in amino acid sequences and positions in the ligand-binding domain in each RXR subtype were found (data not shown). It seems difficult to discuss the difference by docking simulation visually. The results shown in Figure 3, however, revealed a promising binding affinity of compound **8a**, which was docked into the binding site of 1mvc RXR receptor exactly superimposed on the native bound ligand (BMS649: the same as SR11237 (**3**)) with root of mean square deviation (RMSD) of 0.604 Å. Moreover, compound **8a** formed three hydrogen bonds with the same atoms of amino acids Arg^{316} and Ala^{327} as the native ligand, SR11237 (**3**). It should be noticed that the methanesulfonamide moiety is deeply embedded into the lipophilic residue including Leu^{309}, Ile^{310}, and Cys^{432} within distances of 2.99, 2.61, and 3.21 Å, respectively. This close interaction may explain the improper fitting of compound **8a** into the RXR owing to its methanesulfonamide moiety. These results indicate that reduction of molecular lipophilicity is required to produce RXR subtype selectivity and that the introduction of a polar moiety into the linking group should be avoided for the creation of more potent subtype-selective RXR agonists.

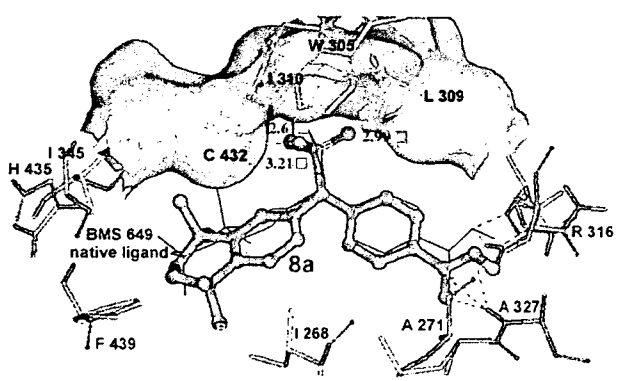

Figure 3. Docking model of compound **8a** (ball and stick, colored by element) in the binding site of RXR (PDB code: 1mvc) using AutoDock3.05. It exhibited 3 H-bonds between Arg^{316} and Ala^{327} (dotted blue lines) with RMSD of 0.604 Å from BMS649 (the same as SR11237 (**3**)), the native ligand.

Several RXR agonists have recently been used in the clinical trial as therapeutic agents against cancer or as chemopreventive agents.[12] Other RXR agonists have also been described as insulin sensitizer or anti obese agents and were shown to decrease blood sugar or weight gain in rodent models.[24,25] Therefore, less lipophilic and subtype-selective RXR agonists we are seeking for are expected to be therapeutic agents for cancer or metabolic syndrome, and may be useful biological tools for elucidating each RXR subtype function.

Conclusions

In this study, we aimed to produce less lipophilic and subtype-selective RXR agonists. By designing sulfonamide-type RXR agonists, 4-[*N*-methanesulfonyl-*N*-(5,5,8,8-tetramethyl-5,6,7,8-tetrahydro-2-naphthyl)amino]benzoic acid (**8a**) was found to prefer RXRα over RXRβ and RXRγ, although the potency is less than the potencies of well-known RXR pan-agonists. Moreover, our results suggest that for production of subtype-preferential RXR agonists, reduction of lipophilicity should be performed at the lipophilic domain of RXR agonists rather than at the acidic domain. In the future, modification of our strategy should enable production of more potent, subtype-selective RXR agonists, which may be useful for elucidation of each RXR subtype function and/or development of RXR drugs with appropriate action spectra.

Experimental Section

Chemistry

Melting points were determined with a Yanagimoto hot-stage melting point apparatus and are uncorrected. IR were recorded on JASCO FT/IR350 (KBr). ^{1}H NMR spectra were recorded on a Var-

ianVXR-300 (300 MHz) or VarianVXR-500 (500 MHz) spectrometer. Elemental analysis was carried out with a Yanagimoto MT-5 CHN recorder elemental analyzer. FAB-MS was carried out with a VG70-SE.

SR11237 (3) and LGD1069 (5). These compounds were prepared according to references [26] and [22], respectively.

5,5,8,8-Tetramethyl-5,6,7,8-tetrahydro-2-naphthylamine (11). This compound was prepared according to reference [7].

Methyl-*N*-(5,5,8,8-tetramethyl-5,6,7,8-tetrahydro-2-naphthyl)-4-aminobenzoate (12). Concentrated H_2SO_4 (1.5 mL) on cooling was added to a solution of 4-iodobenzoic acid (5.0 g, 20 mmol) in dry MeOH (50 mL), and the mixture was held at reflux for 4 h. The reaction mixture was concentrated under reduced pressure and $NaHCO_3$ solution (300 mL) was added to the residue. The mixture was extracted with EtOAc (3×200 mL). After being washed with H_2O (200 mL) and brine (200 mL), the organic layer was dried over $MgSO_4$ and evaporated under reduced pressure to yield methyl 4-iodobenzoate. Recrystallization from CH_2Cl_2 afforded colorless cubes (72–85%); mp: 105.0–106.0 °C; ^{1}H NMR (300 MHz, $CDCl_3$): δ = 7.81 (2H, d, J = 8.5 Hz), 7.75 (2H, d, J = 8.5 Hz), 3.91 ppm (3H, s); IR (KBr): $\tilde{\nu}$ = 1714 cm^{-1}.

Dry toluene (20.0 mL) was added to a mixture of methyl 4-iodobenzoate (2.62 g, 10 mmol), amine **11** (2.03 g, 10 mmol), (±)-BINAP (0.47 g, 0.75 mmol), $Pd_2(dba)_3$ (0.46 g, 0.5 mmol), and Cs_2CO_3 (4.56 g, 14.0 mmol) under argon at room temperature. The mixture was held at reflux for 16 h. The slurry was filtered through Celite, and the Celite cake was washed with EtOAc (500 mL). After being washed with H_2O (2×150 mL) and brine (150 mL), the organic layer was dried over $MgSO_4$ and evaporated under reduced pressure. The residue was purified by silica gel column chromatography (*n*-hexane/EtOAc = 8:1) to afford compound **12**. Recrystallization from CH_2Cl_2/*n*-hexane afforded colorless cubes (85%); mp: > 200 °C; ^{1}H NMR (300 MHz, $CDCl_3$): δ = 7.90 (2H, d, J = 8.5 Hz), 7.27 (1H, d, J = 8.5 Hz), 7.09 (1H, s), 6.96 (1H, d, J = 8.5 Hz), 6.93 (2H, d, J = 9.0 Hz), 3.87 (3H, s), 1.69 (4H, s), 1.28 (6H, s) 1.27 ppm (6H, s); IR (KBr): $\tilde{\nu}$ = 3357, 1693 cm^{-1}.

Methyl-[*N*-(5,5,8,8-tetramethyl-5,6,7,8-tetrahydro-2-naphthyl)]-6-aminonicotinate (13). Compound **11** (610 mg, 3.0 mmol) was added to a solution of 6-chloronicotinic acid (473 mg, 3.0 mmol) in AcOH (3.0 mL), and the mixture was held at reflux for 10 h. The reaction mixture was poured into H_2O (100 mL) and extracted with EtOAc (3×100 mL). After being washed with H_2O (100 mL), the organic layer was dried over $MgSO_4$ and evaporated under reduced pressure. Recrystallization from EtOAc afforded [*N*-(5,5,8,8-tetramethyl-5,6,7,8-tetrahydro-2-naphthyl)]-6-aminonicotinic acid as colorless cubes (633 mg, 60%). ^{1}H NMR (300 MHz, [D$_6$]DMSO): δ = 12.55 (1H, br s), 9.40 (1H, s), 8.64 (1H, d, J = 2.5 Hz), 7.94 (1H, dd, J = 9.0, 2.5 Hz), 7.52 (1H, dd, J = 8.5, 2.5 Hz), 7.43 (1H, d, J = 2.5 Hz), 7.25 (1H, d, J = 8.5 Hz), 6.79 (1H, d, J = 9.0 Hz), 1.64 (4H, s), 1.25 (6H, s), 1.23 ppm (6H, s); FAB-MS *m/z*; 325 [*M*+H]$^+$.

Concentrated H_2SO_4 (0.07 mL) on cooling was added to a solution of [*N*-(5,5,8,8-tetramethyl-5,6,7,8-tetrahydro-2-naphthyl)]-6-aminonicotinic acid (150 mg, 0.6 mmol) in dry MeOH (1.5 mL) and the mixture was held at reflux overnight. The reaction mixture was concentrated under reduced pressure and poured into a sat. $NaHCO_3$ solution (100 mL). The mixture was extracted with EtOAc (2×100 mL). After being washed with H_2O (100 mL) and brine (100 mL), the organic layer was dried over $MgSO_4$ and evaporated under reduced pressure to yield compound **13** (123 mg, 80%). As this compound gave a single spot on TLC, **13** was used for the next step without further purification. ^{1}H NMR (300 MHz, $CDCl_3$): δ = 8.79 (1H, d, J = 2.5 Hz), 8.04 (1H, dd, J = 9.0, 2.5 Hz), 7.37 (1H, s), 7.32 (1H, d, J = 8.5 Hz), 7.20 (1H, d, J = 2.5 Hz), 7.10 (1H, dd, J = 8.5, 2.5 Hz), 6.80 (1H, d, J = 9.0 Hz), 3.89 (3H, s), 1.70 (4H, s), 1.29 (6H, s), 1.28 ppm (6H, s); FAB-MS *m/z*; 339 [*M*+H]$^+$.

Ethyl-[*N*-(2,5,5,8,8-tetramethyl-5,6,7,8-tetrahydro-2-naphthyl)]-2-amino-pyrimidine carboxylate (14). This compound was prepared according to references [15] and [16].

General procedure for the synthesis of *N*-alkylsulfonamide intermediates. The corresponding intermediates (**12–14**) (1.0 mmol) were added to a DMF solution (5.0 mL) containing sodium hydride (2.5 mmol, 60% purity in oil) under argon at room temperature for 5 min. Then, a corresponding alkylsulfonyl chloride (1.2 mmol) was added to the solution. After stirring for 2 h, the mixture was poured into H_2O, and extracted with EtOAc. The organic phase was washed with H_2O and brine and then dried over $MgSO_4$ and concentrated under reduced pressure. The residue was purified by silica gel flash chromatography to afford *N*-alkylsulfonamide intermediates.

General procedure for the synthesis of [*N*-alkylsulfonyl-*N*-(5,5,8,8-tetramethyl-5,6,7,8-tetrahydro-2-naphthyl)]-4-aminobenzoic acids (8a–d). LiOH·H_2O (2.0 mmol) was added to a solution of *N*-alkylsulfonamide intermediates (1.0 mmol) in THF/H_2O (2.0 mL, 3:1) and the mixture was kept at room temperature over night. The mixture was poured into 2 N HCl (15.0 mL) and extracted with EtOAc (3×20 mL). After being washed with H_2O (30 mL) and brine (30 mL), the organic layer was dried over $MgSO_4$ and evaporated under reduced pressure. Recrystallization gave the target molecules **8a–d**.

[*N*-Methanesulfonyl-*N*-(5,5,8,8-tetramethyl-5,6,7,8-tetrahydro-2-naphthyl)]-4-aminobenzoic acid (8a). Colorless needles from EtOAc/*n*-hexane; mp: 165.0–166.0 °C; Yield 71%; ^{1}H NMR (300 MHz, [D$_6$]DMSO): δ = 12.98 (1H, br s), 7.94 (2H, d, J = 8.5 Hz), 7.44 (1H, dd, J = 8.5, 2.5 Hz), 7.40 (1H, d, J = 8.5 Hz), 7.37 (1H, d, J = 2.5 Hz), 7.18 (2H, d, J = 8.5 Hz), 3.33 (3H, s), 1.64 (4H, s), 1.25 (6H, s), 1.22 ppm (6H, s); IR (KBr): $\tilde{\nu}$ = 2962–2800, 1687 cm^{-1}; FAB-MS *m/z*; 401 [*M*]$^+$, 402 [*M*+H]$^+$; Anal. Calcd for $C_{22}H_{27}NO_4S$: C, 65.81; H, 6.78; N, 3.49. Found: C, 65.77; H, 6.61; N, 3.41.

[*N*-Ethanesulfonyl-*N*-(5,5,8,8-tetramethyl-5,6,7,8-tetrahydro-2-naphthyl)]-4-aminobenzoic acid (8b). Colorless columns from CH_2Cl_2/*n*-hexane; mp: 167.0–168.0 °C; Yield 43%; ^{1}H NMR (300 MHz, [D$_6$]DMSO): δ = 13.00 (1H, br s), 7.92 (2H, d, J = 9.0 Hz), 7.44 (2H, d, J = 9.0 Hz), 7.42 (1H, d, J = 8.5 Hz), 7.36 (1H, d, J = 2.5 Hz), 7.18 (1H, dd, J = 8.5, 2.5 Hz), 3.42 (2H, q, J = 7.5 Hz), 1.64 (4H, s), 1.31 (3H, t, J = 7.5 Hz), 1.25 (6H, s), 1.22 ppm (6H, s); IR (KBr): $\tilde{\nu}$ = 1719, 1335, 1139 cm^{-1}; FAB-MS *m/z*; 415 [*M*]$^+$, 416 [*M*+H]$^+$; Anal. Calcd for $C_{23}H_{29}NO_4S$: C, 66.48; H, 7.03; N, 3.37. Found: C, 66.28; H, 6.97; N, 3.46.

[*N*-*n*-Propanesulfonyl-*N*-(5,5,8,8-tetramethyl-5,6,7,8-tetrahydro-2-naphthyl)]-4-aminobenzoic acid (8c). Colorless needles from CH_2Cl_2/*n*-hexane; mp: 201.0–203.0 °C; Yield 32%; ^{1}H NMR (300 MHz, [D$_6$]DMSO): δ = 12.94 (1H, br s), 7.92 (2H, d, J = 9.0 Hz), 7.44 (2H, d, J = 9.0 Hz), 7.39 (1H, d, J = 8.5 Hz), 7.35 (1H, d, J = 2.0 Hz), 7.18 (1H, dd, J = 8.5, 2.0 Hz), 3.39 (2H, t, J = 7.5 Hz), 1.79 (2H, sex, J = 7.5 Hz), 1.64 (4H, s), 1.24 (6H, s) 1.22 (6H, s), 1.00 ppm (3H, t, J = 7.5 Hz); IR (KBr): $\tilde{\nu}$ = 1688, 1329, 1148 cm^{-1}; FAB-MS *m/z*; 430 [*M*+H$^+$]; Anal. Calcd for $C_{24}H_{31}NO_4S$: C, 67.01; H, 7.27; N, 3.26. Found: C, 67.00; H, 7.20; N, 3.44.

[*N*-*n*-Butanesulfonyl-*N*-(5,5,8,8-tetramethyl-5,6,7,8-tetrahydro-2-naphthyl)]-4-aminobenzoic acid (8d). White needles from CH_2Cl_2/

n-hexane; mp: 213.0–215.0 °C; Yield 38%; ^{1}H NMR (300 MHz, [D$_6$]DMSO): δ = 13.01 (1H, br s), 7.92 (2H, d, J = 9.0 Hz), 7.44 (2H, d, J = 9.0 Hz), 7.39 (1H, d, J = 8.5 Hz), 7.35 (1H, d, J = 2.0 Hz), 7.18 (1H, dd, J = 8.5, 2.0 Hz), 3.42 (2H, t, J = 7.5 Hz), 1.73 (2H, sex, J = 7.5 Hz), 1.64 (4H, s), 1.42 (2H, m), 1.24 (6H, s), 1.22 (6H, s), 0.88 ppm (3H, t, J = 7.5 Hz); IR (KBr): $\tilde{\nu}$ = 1688, 1332, 1173 cm^{-1}; FAB-MS *m/z*; 443 [*M*]$^+$, 444 [*M*+H]$^+$; Anal. Calcd for $C_{25}H_{33}NO_4S$: C, 67.69; H, 7.50; N, 3.16. Found: C, 67.35; H, 7.31; N, 3.12.

[*N*-Methanesulfonyl-*N*-(5,5,8,8-tetramethyl-5,6,7,8-tetrahydro-2-naphthyl)]-6-aminonicotinic acid (9). Colorless needles from CH_2Cl_2/*n*-hexane; mp: 228.0–228.5 °C; Yield 89%; ^{1}H NMR (300 MHz, [D$_6$]DMSO): δ = 8.89 (1H, d, J = 2.5 Hz), 8.16 (1H, dd, J = 8.5, 2.5 Hz), 7.45 (2H, d, J = 8,5 Hz), 7.33 (1H, d, J = 2.5 Hz), 7.12 (1H, dd, J = 8.5 Hz, 2.5 Hz), 6.63 (1H, d, J = 8.5 Hz), 3.59 (3H, s), 1.67 (4H, s), 1.28 (6H, s), 1.23 ppm (6H, s); IR (KBr): $\tilde{\nu}$ = 1690, 1366, 1171 cm^{-1}; FAB-MS *m/z*; 403 [*M*+H]$^+$; Anal. Calcd for $C_{21}H_{26}N_2O_4S$: C, 62.66; H, 6.51; N, 6.96. Found: C, 62.62; H, 6.29; N, 6.55.

[*N*-Methanesulfonyl-*N*-(5,5,8,8-tetramethyl-5,6,7,8-tetrahydro-2-naphthyl)]-2-amino-pyrimidine carboxylic acid (10). White cubes from EtOAc/*n*-hexane; mp: 248.0–250.0 °C; Yield 87%; ^{1}H NMR (300 MHz, $CDCl_3$): δ = 9.13 (2H, s), 7.39 (1H, d, J = 8,5 Hz), 7.17 (1H, d, J = 2.5 Hz), 7.04 (1H, dd, J = 8.5 Hz, 2.5 Hz), 3.63 (3H, s), 1.71 (4H, s), 1.31 (6H, s), 1.27 ppm (6H, s); IR (KBr): $\tilde{\nu}$ = 1696, 1369, 1173 cm^{-1}; FAB-MS *m/z*; 404 [*M*+H]$^+$; Anal. Calcd for $C_{20}H_{25}N_3O_4S$: C, 59.53; H, 6.25; N, 10.41. Found: C, 59.52; H, 6.33; N, 10.53.

Calculation of Clog*P* values. Log*P* values for compounds were calculated with ChemDraw Ultra 7.0 or software available from molinspiration (http://www.molinspiration.com/).

NBT reduction assay

Culture of HL-60 cells. The human promyelocyte leukemia cell line HL-60 was cultured in RPMI1640, which contained 10% fetal bovine serum (FBS) and antibiotics (2% of penicillin-streptomycin solution purchased from SIGMA), in a humidified atmosphere of 5% CO_2 at 37 °C.

NBT reduction assay.[13,17,18] Test compounds were dissolved in DMSO at 20 mM for stock solutions. To a suspension of cells at a concentration of 8×10^4 cells mL^{-1} was added a test compound solution in DMSO. Final DMSO concentration was kept below 0.1%. For a vehicle and a positive control, the same volume of DMSO and Am80[7] solution in DMSO were added, respectively. After incubation for 4 days, NBT reduction assay was performed as described below. Cells were incubated in RPMI1640 (10% FBS) and an equal volume of phosphate-buffer saline (PBS (−)) containing 0.2 *w/w*% NBT and 12-*O*-tetradecanoylphorbol-13-acetate (TPA, 200 ng mL^{-1}) in a humidified atmosphere of 5% CO_2 at 37 °C for 30 min. The rate of cell differentiation was calculated by the percentage of cells containing blue–black formazan using more than 200 cells. Average of at least three results for each assay was calculated. Synergistic activities of test compounds with Am80 were evaluated in the presence of 3.3×10^{-10} M of Am80, which induces less than 10% of cell differentiation, according to the method described above.

Luciferase reporter gene assay

Culture of COS-1 cells. COS-1 cells were maintained in Dulbecco's modified Eagle's medium supplemented with 10% FBS in a humidified atmosphere of 5% CO_2 at 37 °C.

Luciferase reporter gene assay.[15,19,20] Luciferase reporter gene assays were performed using COS-1 cells transfected with three kinds of vectors; each RXR subtype, a luciferase reporter gene under the control of the appropriate RXR response elements, and secreted alkaline phosphatase (SEAP) gene as a background. A CRBPII-tk-Luc reporter and plasmid DNAs were purified by a QIA filter Plasmid Midi kit. COS-1 cells were transfected with QIA Effectene Transfection reagent according to the supplier's protocol. Test compound solutions whose DMSO concentrations were below 1% were added to the suspension of transfected cells, which were seeded at about 2×10^5 cells mL^{-1} in 96-well white plates. For vehicle and positive control, the same volume of DMSO and 9-*cis*RA solution in DMSO were added, respectively. After incubation in a humidified atmosphere of 5% CO_2 at 37 °C for 18 h, the parts of the medium were used for SEAP and the remaining cells were used for luciferase reporter gene assays with a Steady-Glo Luciferase Assay system (Promega) according to the supplier's protocol. The luciferase activities were normalized using secreted alkaline phosphatase (SEAP) activities. The assays were carried out in duplicate three times.

Molecular docking

The crystal structure of the human RXRα–ligand binding domain (PDB code: 1mvc) was retrieved from the Brookhaven Protein Data Bank: http://www.rcsb.org/pdb/Wecome.do accessed in December 10, 2005. Polar hydrogen atoms were added to both the protein and the ligand. United atom Kollman charges were assigned for the protein. The 3D structures of ligands used for the docking study were constructed by using Chem3D Ultra 8.0 software [Molecular Modeling and Analysis; Cambridge Soft Corporation, USA (2003)]. These ligands were energetically minimized by using MOPAC (semi-empirical quantum mechanics) with AM1 MOZYME geometry. The AutoDock3.05 molecular docking program[23] was employed by using a genetic algorithm with local search (GALS). One hundred individual GA runs, 150 chromosomes, a crossover ratio of 0.80, a rate of gene mutation of 0.02, and an elitism ratio of 0.10 were used for each ligand. The grid box was created with dimensions of $60\times60\times60$ Å^3 which encloses the original ligand BMS649 (SR11237 (**3**)). The box spacing was 0.3 Å. Accelrys Discovery Studio version 1.6 [Accelrys inc., San Diego, CA (2006)] was used for molecular modeling, and the mode of interaction of BMS649 (SR11237 (**3**)) against 1 mvc was used as a standard docked model as well as for RMSD calculation.

Acknowledgements

The authors are grateful to the SC NMR Laboratory of Okayama University for the NMR experiment. This research was partially supported by a Grant-in Aid for Scientific Research on Priority Areas from the Ministry of Education, Science, Culture and Sports of Japan (No. 17790090) and the subsidy to promote science and technology in the prefectures where nuclear power plants and other power plants are located. The authors are also grateful to Mr. Masahiro Yamaguchi and Ms. Sarina Yamaguchi for helpful discussion in the preparation of this manuscript.

Keywords: docking simulations · RXR agonists · subtype preference · subtype selectivity · sulfonamides · synergistic effects

[1] V. Giguère, *Endocr. Rev.* **1999**, *20*, 689–725.
[2] D. J. Mangelsdorf, C. Thummel, M. Beato, P. Herrlich, G. Schütz, K. Umesono, B. Blumberg, P. Kastner, M. Mark, P. Chambon, R. M. Evans, *Cell* **1995**, *83*, 835–839.
[3] G. Benoit, M. Malewicz, T. Perlmann, *Trends Cell Biol.* **2004**, *14*, 369–376.
[4] R. A. Heyman, D. J. Mangelsdorf, J. A. Dyck, R. B. Stein, G. Eichele, R. M. Evans, C. Thaller, *Cell* **1992**, *68*, 397–406.
[5] P. F. Egea, A. Mitschler, D. Moras, *Mol. Endocrinol.* **2002**, *16*, 987–997.
[6] D. J. Mangelsdorf, R. M. Evans, *Cell* **1995**, *83*, 841–850.
[7] H. Kagechika, E. Kawachi, Y. Hashimoto, T. Himi, K. Shudo, *J. Med. Chem.* **1988**, *31*, 2182–2192.
[8] L. Eyrolles, H. Kagechika, E. Kawachi, H. Fukasawa, T. Iijima, Y. Matsushima, Y. Hashimoto, K. Shudo, *J. Med. Chem.* **1994**, *37*, 1508–1517.
[9] C. J. Grubbs, D. L. Hill, K. I. Bland, S. W. Beenken, T. H. Lin, I. Eto, V. R. Atigadda, K. K. Vines, W. J. Brouillette, D. D. Muccio, *Cancer Lett.* **2003**, *201*, 17–24.
[10] W-C. Yen, M. R. Corpuz, R. Y. Prudente, T. A. Cooke, R. P. Bissonnette, A. Negro-Vilar, W. W. Lamph, *Clin. Cancer Res.* **2004**, *10*, 8656–8664.
[11] A. Szanto, V. Narkar, Q. Shen, I. P. Uray, P. J. A. Davies L. Nagy, *Cell Death Differ.* **2004**, *11*, S126–143.
[12] S. M. Lippman R. Lotan, *J. Nutr.* **2000**, *130*, 479–482.
[13] H. Kagechika, K. Shudo, *J. Med. Chem.* **2005**, *48*, 5875–5883.
[14] F. C. Zusi, M. V. Lorenzi, V. Vivat-Hannah, *Therapeutic focus* **2002**, *7*, 1165–1174.
[15] K. Ohta, E. Kawachi, N. Inoue, H. Fukasawa, Y. Hashimoto, A. Itai, H. Kagechika, *Chem. Pharm. Bull.* **2000**, *48*, 1504–1513.
[16] A. Takamizawa, K. Tokuyama, H. Satoh, *Yakugaku Zasshi* **1959**, *79*, 664–669.
[17] S. J. Collins, F. W. Ruscetti, R. E. Gallagher, R. C. Gallo, *J. Exp. Med.* **1979**, *149*, 969–974.
[18] T. Takuma, K. Takeda, K. Konno, *Biochem. Biophys. Res. Commun.* **1987**, *145*, 514–521.
[19] K. Umesono, K. K. Murakami, C. C. Thompson, R. M. Evans, *Cell* **1991**, *65*, 1255–1266.
[20] S. R. Kain, *Methods Mol. Biol.* **1997**, *63*, 49–60.
[21] J. M. Lehmann, L. Jong, A. Fabjul, J. F. Cameron, X. P. Lu, P. Haefner, M. I. Dawson, M. Pfahl, *Science* **1992**, *258*, 1944–1946.
[22] M. F. Boehm, L. Zhang, L. Zhi, M. R. McClurg, E. Berger, M. Wagoner, D. E. Mais, C. M. Suto, P. J. A. Davies, R. A. Heyman, A. M. Nadzan, *J. Med. Chem.* **1995**, *38*, 3146–3155.
[23] G. M. Morris, D. S. Goodsell, R. S. Halliday, R. Huey, W. E. Hart, R. K. Belew, A. J. Olson, *J. Comput. Chem.* **1998**, *19*, 1639–1662.
[24] R. Mukherjee, P. J. A. Davies, D. L. Crombie, E. D. Bischoff, R. M. Cesario, L. Jow, L. G. Hamann, M. F. Boehm, C. E. Mondon, A. M. Nadzan, J. R. Paterniti, Jr., R. A. Heyman, *Nature* **1997**, *386*, 407–410.
[25] Y-L. Liu, M. V. Sennitt, D. C. Hislop, D. L. Crombie, R. A. Heyman, M. A. Cawthorne, *Int. J. Obes.* **2000**, *24*, 997–1004.
[26] M. Pfahl, X. K. Zhang, J. M. Lehmann, M. I. Dawson, J. F. Cameron, P. D. Hobbs, L. Jong, PCT Int. Appl. 9412880, **1994**.

Received: September 22, 2007
Published online on December 21, 2007

Colloid Polym Sci
DOI 10.1007/s00396-008-1837-7

ORIGINAL CONTRIBUTION

Preparation of monodisperse crosslinked polymelamine microcapsules by phase separation method

Eiji Kamio · Aiko Kato · Satoshi Yonemura · Tsutomu Ono · Hidekazu Yoshizawa

Received: 16 August 2007 / Revised: 21 December 2007 / Accepted: 24 December 2007

Abstract Monodisperse polymelamine microcapsules were prepared by phase separation method. Control of microcapsule diameter was investigated using the uniform-sized oil-in-water emulsion droplets as the capsule core. The monodisperse emulsion droplets were prepared using the Shirasu porous glass (SPG) membrane emulsification technique. The effects of the diameter of the oil droplet and concentration of sodium dodecyl sulfate (SDS), which is a typical emulsifier in SPG membrane emulsification, on microencapsulation were investigated. The microcapsules were aggregated when oil droplets with small size were microencapsulated at high SDS concentration. To reduce the SDS concentration, the creamed emulsion was used. The monodisperse polymelamine microcapsules were successfully prepared by using the creamed emulsion. The microcapsule diameter was almost similar to the diameter of the encapsulated oil droplet. The coefficient of variation values was about 10% for all microcapsules prepared in this study. Control of microcapsule diameter was achieved in the range of 5–60 μm.

Keywords Monodisperse microcapsule · Phase separation method · Control of capsule diameter · Shirasu porous glass membrane · Sodium dodecyl sulfate concentration

E. Kamio · A. Kato · S. Yonemura · T. Ono (✉) · H. Yoshizawa
Department of Environmental Chemistry and Materials,
Okayama University,
3-1-1, Tsushima-naka, Okayama-shi,
Okayama 700-8530, Japan
e-mail: tono@cc.okayama-u.ac.jp

Introduction

Microcapsules are tiny packaged materials that have been used in a wide variety of fields such as in chemical and pharmaceutical industries and in cosmetics and printing. In the 1950s, they were used in carbonless copy paper developed by the National Cash Register Company [1]. The microcapsules in the carbonless copy paper were powder-like substances that protected the core material from damage caused by oxidation and rough handling and treatment. Several microencapsulation methods were subsequently developed and applied in the fields in which they are used today. Microcapsules with a variety of functions can be produced by using different microencapsulation methods.

Of the several microencapsulation methods, the phase separation method is one of the most useful. Crosslinked polyamino resin microcapsules prepared by phase separation method are mono-core microcapsules that enclose water-insoluble organic solvents. They have smooth, thin, and transparent membranes. The capsule membrane is formed at the liquid–liquid interface of an oil-in-water (O/W) emulsion from a continuous phase. These characteristics are suitable for the preparation of a microcapsule that encloses an organic solvent with electrophoretic microparticles, which is used as an element of paper-like display systems [2–4]. However, there are still some problems in applying the microcapsule prepared by the phase separation method to the paper-like display system. Controlling the diameter of the microcapsule is one of the most serious technical issues. The diameter of the microcapsule directly affects the thickness of the display. It also affects the intensity of the electric field and the electrophoretic performance of the microparticles in the microcapsule. In

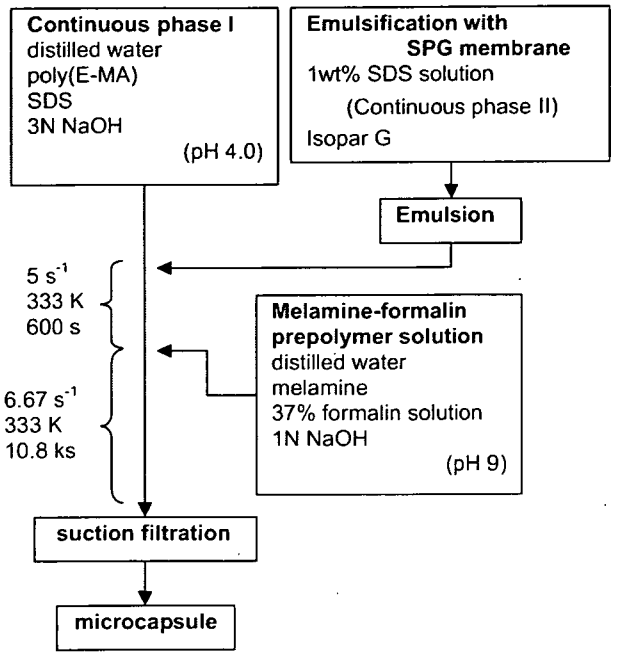

Fig. 1 Protocol for the preparation of monodisperse crosslinked polymelamine microcapsules

Table 1 Preparation condition of crosslinked polymelamine microcapsules

	Total amount (g)	Content	Amount (g)
(A)			
Continuous phase I	77.5	Distilled water (+ NaOH)	67.5
		Poly(E-MA)	2.5
Emulsion	37.5	Isopar G	15.0
		Continuous phase II[a]	30.0
Melamine–formalin prepolymer solution	50	Melamine	5.0
		37% formalin solution	12.5
		Distilled water (+ NaOH)	32.5
(B)			
Continuous phase I	92.5	Distilled water (+ NaOH)	90.0
		Poly(E-MA)	2.5
Creamed emulsion	22.5	Isopar G	15.0
		Continuous phase II[a]	7.5
Melamine–formalin prepolymer solution	50	Melamine	5.0
		37% formalin solution	12.5
		Distilled water (+ NaOH)	32.5

Microencapsulation was carried out with (A) emulsion in state of SPG emulsification and (B) creamed emulsion.
[a] Continuous phase II is 0.5 wt.% SDS solution.

Table 2 Preparation condition of crosslinked polymelamine microcapsules with different amounts of oil phase

	Continuous phase I[a]			Emulsion[b]				Prepolymer solution[c] (g)	Poly(E-MA)/total surface area (g/m^2)
	Total (g)	Content (g)		Total (g)	Content (g)				
		Poly(E-MA)	SDS		Oil phase	Aqueous phase			
(A)	96	2.5	0.14	5	1	4		50	3.17
(B)	92	2.5	0.13	10	2	8		50	1.58
(C)	80	2.5	0.11	25	5	20		50	0.63
(D)	60	2.5	0.07	50	10	40		50	0.32

[a] Solvent was distilled water and its pH was adjusted with 3×10^3 mol/m^3 NaOH solution to 4.0.
[b] Emulsion was prepared using SPG membrane with 2.6-μm diameter pore. Aqueous phase (continuous phase II) was 0.2 wt.% SDS solution.
[c] Composition was 5.0 g of melamine, 12.5 g of 37% formalin solution, and 32.5 g of distilled water with its pH adjusted with 1×10^3 mol/m^3 NaOH solution to 9.0.

Table 3 Preparation conditions of crosslinked polymelamine microcapsules at different SDS concentrations

	Total amount (g)	Content	Amount (g)[a]		
			(1)	(2)	(3)
Continuous phase I	90	Distilled water (+ NaOH)	87.30	87.07	86.85
		Poly(E-MA)	2.5	2.5	2.5
		SDS	0.20	0.43	0.65
Creamed emulsion[b]	25	Isopar G	15.0	15.0	15.0
		Continuous phase II	10.0	10.0	10.0
Melamine–formalin prepolymer solution	50	Melamine	5.0	5.0	5.0
		37% formalin solution	12.5	12.5	12.5
		Distilled water (+ NaOH)	32.5	32.5	32.5

[a] Panels (1), (2), and (3) correspond to the conditions (1), (2), and (3) in Fig. 6.

[b] Emulsion was prepared using SPG membrane with 4.8-μm diameter pore. Continuous phase II was 1 wt.% SDS solution.

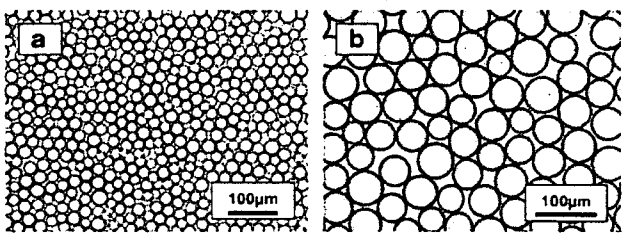

Fig. 2 Optical microscope photographs of emulsions prepared using SPG membrane. SPG membrane pore sizes were **a** 4.8 μm and **b** 13 μm

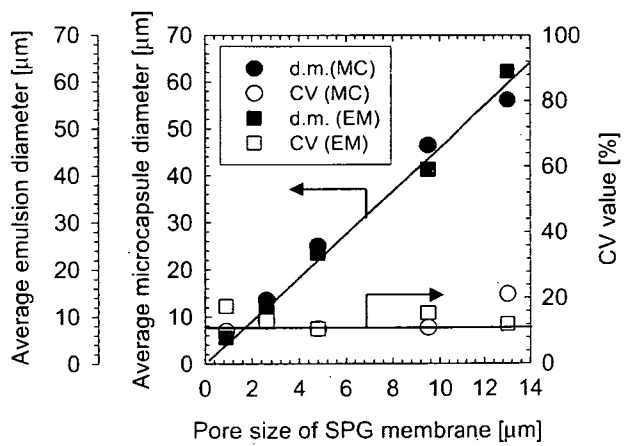

Fig. 3 Relationships between average emulsion droplet and microcapsule diameters and pore size of SPG membrane. *MC* Microcapsule, *EM* emulsion droplet, *d.m.* diameter

addition, to closely pave an electrode with microcapsules, the microcapsules must have a uniform diameter.

A few researchers have reported on controlling the diameter of a microcapsule prepared by phase separation method [5–8]. They reported that the microcapsule diameter

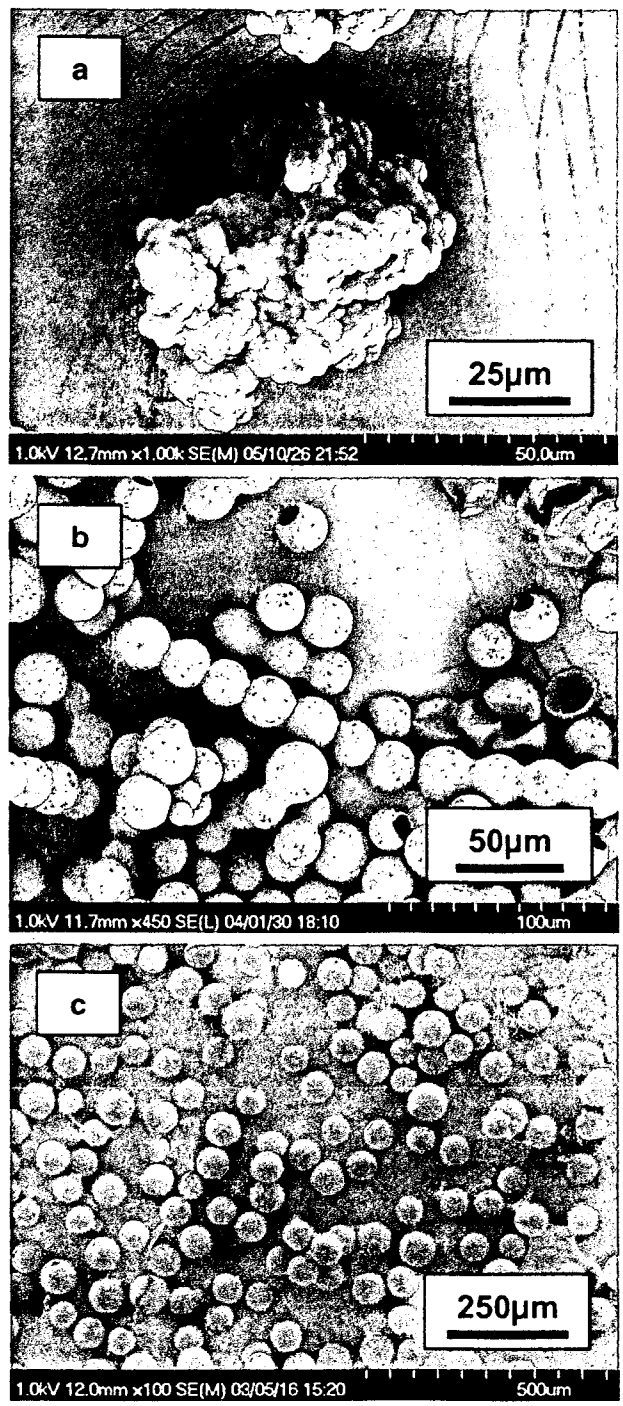

Fig. 4 SEM observations of microcapsules prepared in conditions shown in Table 1(A). Average diameters of emulsion droplets used as core were **a** 5.5 μm, **b** 23 μm, and **c** 62 μm

was controlled by adjusting stirring speed during the microencapsulation process and that the average diameter of the microcapsules decreased as stirring speed increased. However, the prepared microcapsules were not monodisperse ones.

The objective of our work was to implement a technique that controls the diameter of crosslinked polymelamine microcapsules prepared by phase separation method. We tried to fabricate microcapsules with a desired capsule diameter in a narrow size distribution. We used the Shirasu porous glass (SPG) membrane emulsification technique to control the diameter of a microcapsule.

Experimental

Reagents

Melamine and 37% formalin solution were used as the monomer and the condensing agent, respectively. Sodium dodecyl sulfate (SDS) was used as an emulsion stabilizer. Sodium hydroxide was used to adjust the pH of the continuous phase of the microencapsulation process (hereafter called continuous phase I). All of these analytical grade reagents were purchased from Wako Pure Chemical Industry, Ltd. The polymeric surfactant, poly(ethylene-*alt*-maleic anhydride) (poly(E-MA)), was purchased from Aldrich Co. Ltd. Isopar G, the core material of the microcapsule, was purchased from Exxon Mobil Co.

SPG membrane emulsification

The SPG membrane is highly porous and is made from deposits of volcanic ash and sand. SPG membranes have a huge number of pores of uniform micron size. One can select an SPG membrane of a desired pore size to prepare the O/W emulsions with uniform-sized oil droplets [9–15]. We used tubular SPG membranes with 0.9, 2.6, 4.8, 9.5, and 13-μm pores. An SPG membrane emulsification module (SPG mini-kit, SPG Technology Co. Ltd.) was used to prepare the O/W emulsions with uniform-sized oil droplets. First, the continuous phase of the emulsification process (hereafter called continuous phase II) was introduced inside the SPG membrane. The oil phase was inserted into the continuous phase II from the outside of the SPG membrane by compressed N_2 gas at a pressure that was kept constant during the emulsification process. The resulting emulsion was circulated inside the SPG membrane using a pump. In this study, an aqueous solution dissolving a desired amount of SDS was used as continuous phase II.

Preparation of crosslinked polymelamine microcapsule

Crosslinked polymelamine microcapsules were prepared with the following procedure. An aqueous solution containing poly(E-MA) was used as continuous phase I. Its pH was adjusted to 4.0 with 3×10^3 mol/m^3 NaOH aqueous solution. The emulsion prepared by using the SPG membrane was added to a desired amount in continuous

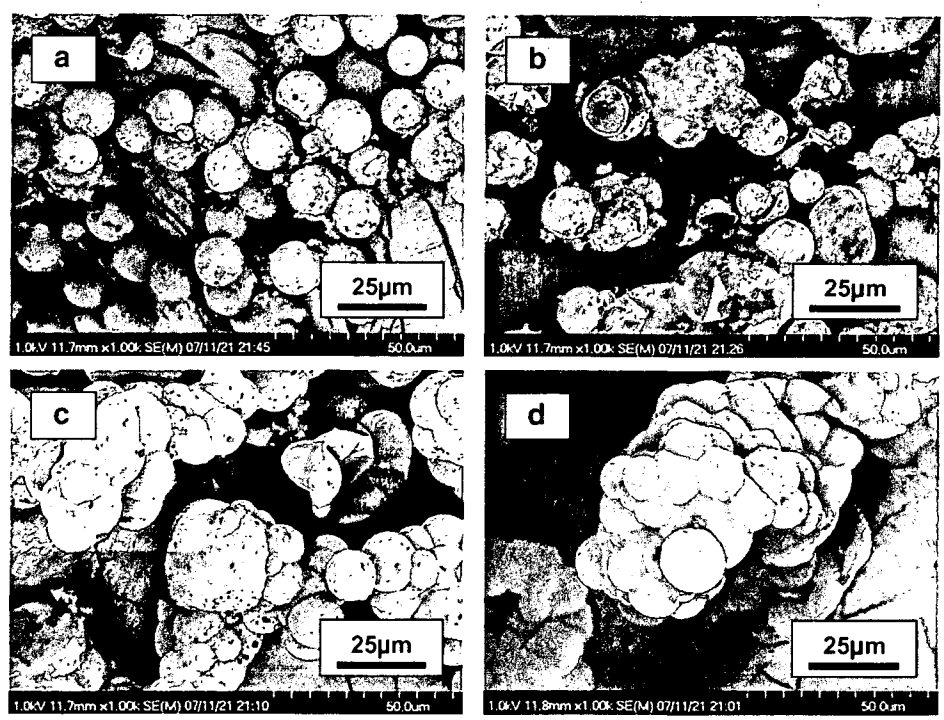

Fig. 5 SEM observations of microcapsules prepared with various amounts of emulsion droplet. The total amount of the oil phase: **a** 1.0 g, **b** 2.0 g, **c** 5.0 g, and **d** 10.0 g. The average diameter of the encapsulated emulsion droplet was 13 μm

phase I. The mixture was stirred for 600 s at 333 K under agitation at 5 s^{-1}. Then, microencapsulation was started by adding the melamine–formalin prepolymer solution, which was prepared separately. The prepolymer solution was prepared as follows: 5.0 g of melamine, 12.5 g of formalin solution, and 32.5 g of distilled water with an adjusted pH of 9 with 1×10^3 mol/m^3 NaOH aqueous solution were mixed and stirred at 333 K for 900 s. During the microencapsulation, the temperature was kept constant at 333 K. The microencapsulation was carried out for 10.8 ks under agitation at 6.67 s^{-1}. After 10.8 ks, the prepared microcapsules were collected by suction filtration and washed with distilled water. The morphology of the microcapsules was observed by a field emission scanning electron microscope (FE-SEM S-4700, Hitachi).

The preparation process of the crosslinked polymelamine microcapsule is shown in Fig. 1. The preparation conditions are summarized in Tables 1, 2, and 3.

Results and discussion

Figure 2 shows the O/W emulsion prepared using the SPG membrane emulsification technique. As shown in Fig. 2, the size of the prepared oil droplets was uniform. The average diameter and the coefficient of variation (CV) value of the emulsion droplets prepared using the SPG membranes with several pore sizes are summarized in Fig. 3. The average diameters of the emulsion droplets were in proportion to the pore diameters of the SPG membrane. They were about five times as large as the pore diameters. The CV values were almost 10%. Until now, some researchers reported the relationship between the pore diameter of SPG membrane and the diameter of the emulsion droplet. For example, Nakashima and Shimizu reported that the diameter of the kerosene droplet was 3.25 times as large as the pore diameter of the SPG membrane [13]. Omi et al. reported that the droplet diameter of the mixture of styrene–divinylbenzene–hexadecane and the mixture of benzene and hexadecane were linear to the pore size of the SPG membrane with slopes of 6.62 and 5.2, respectively [14]. Shiomori et al. reported that the diameter of the oil droplet of isooctane containing olive oil was proportional to the pore diameter of the SPG membrane with a slope of 3.4 [15]. These results show a validity of the result in this study. If the obtained emulsion droplet is not destroyed during the microencapsulation process and the capsule membrane is successfully formed, a microcapsule with the same diameter and size distribution as the used emulsion droplet can be prepared.

In our first investigation, we attempted to prepare microcapsules by adding the emulsion, which was in the emulsification state, to continuous phase I. The microencapsulation conditions are shown in Table 1(A). As a result, the microencapsulation was strongly influenced by the diameter of the emulsion droplet: the microcapsules aggregated with each other when the diameter of the

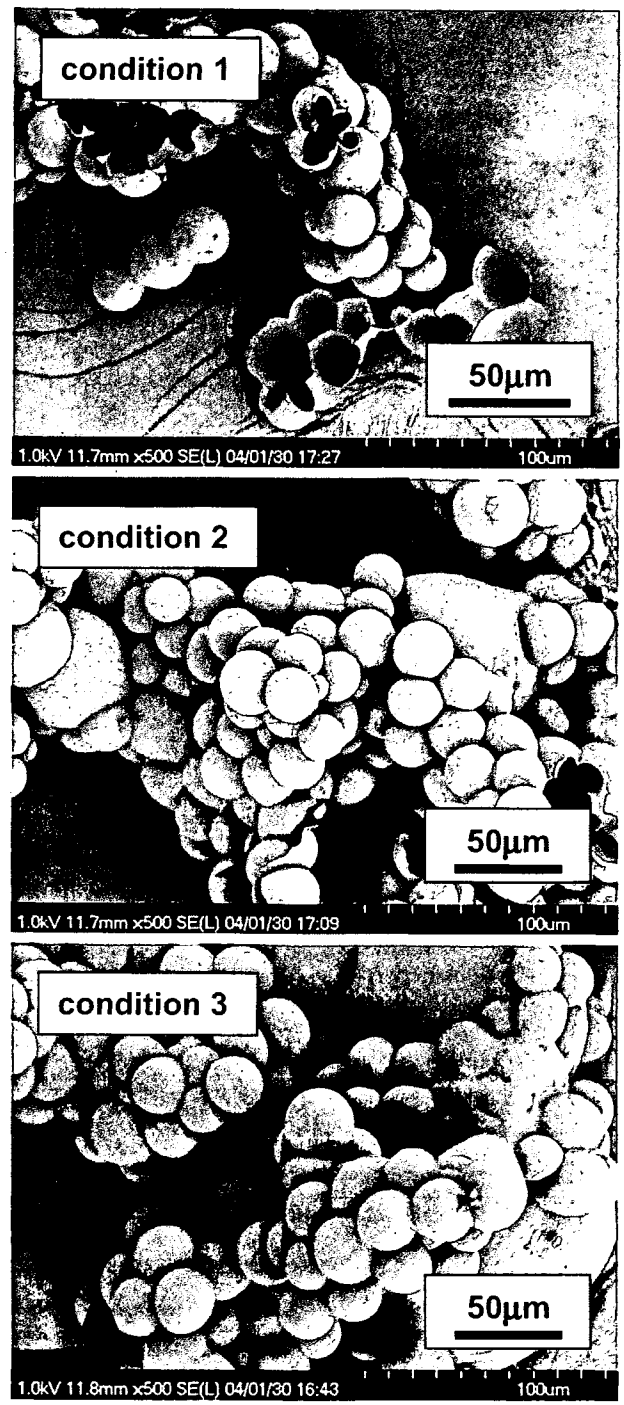

Fig. 6 SEM observations of microcapsules prepared in conditions shown in Table 2. Emulsion was prepared using an SPG membrane with a pore size of 4.8 μm. Average diameter of emulsion droplets was 23 μm. SDS concentration in continuous phase III was 0.2 wt.% (condition 1), 0.35 wt.% (condition 2), and 0.5 wt.% (condition 3)